DOI: 10.13009/EUCASS2019-592

DOI: 592

Evaluation of Thermo-Acoustic Stability Behavior in Full-Scale Liquid Rocket Propulsion Systems

S. Koeglmeier⋆ and R. Kaess
ArianeGroup GmbH
München, D-81611, Germany
stefan.koeglmeier@ariane.group · roland.kaess@ariane.group
⋆Corresponding author

Abstract

Owing to the lack of predictive analysis methods the evaluation of combustion stability characteristics by means of full-scale testing is still the central element of the industrial development process for liquid rocket propulsion systems. This publication reports on current tools and techniques used to assess the thermo-acoustic stability behavior by means of dynamic combustion chamber pressure measurements. Special emphasis is placed on the application of so-called infinite tube pressure probes as a means for attaining high quality measurement data under the constrains of full-scale testing.

1. Introduction

Thermo-acoustic instabilities in liquid rocket propulsion systems may be characterized as an unsteady combustion phenomenon which manifests as large amplitude pressure oscillations of relatively high frequency. Associated with the latter are often massively increased heat transfer rates to the walls of the combustion chamber and severe mechanical vibrations, both capable of causing catastrophic failure of the entire propulsion system. A significant number of liquid rocket development programs have been affected by this problem where the most famous example is certainly the F1 engine for the first stage of the Apollo Saturn V vehicle. The development involved more than 3200 full-scale tests where most of these tests where carried out in order to solve the problems arising from combustion instability.[5] The failure of the second Ariane I flight in May 1980 is probably the most disastrous case of combustion instability in the European rocket propulsion history. Here, one of the first stage SEP Viking 5 motors produced spontaneous instabilities after lift-off which finally resulted in a complete failure of the entire mission. The consequence of this incident was an expensive re-design and certification program which grounded the vehicle for more than one year.[9]

Since the early studies of Rayleigh[17] it is well known that thermo-acoustic instabilities result from an interaction between heat-release fluctuations (originating from the combustion process) and the acoustics of the confinement, i.e. the combustion chamber. Mathematically speaking, the criterion under which an instability may arise is given by the following inequality:*

$$\text{INSTABILITY} \quad \Leftrightarrow \quad \frac{\gamma - 1}{\varrho c^2} \iiint_{\Omega} \langle p' \dot{q}' \rangle dV - \iint_{\partial\Omega} \langle n_i I_i \rangle dA \; > \; 0 \tag{1}$$

where $\langle \cdot \rangle$ is the operator of local temporal average and p' and $\dot{q}'$ denote the instantaneous pressure and heat release fluctuation inside the combustion chamber domain Ω, respectively. Moreover, γ is the ratio of specific heats, ϱ the mean density, c the sonic velocity and n_i the normal vector to the system boundary $\partial\Omega$. I_i represents the instantaneous acoustic energy flux over the latter. The volume integral represents the coupling between heat-release and acoustic pressure fluctuations, the surface integral the loss of acoustic energy over the system boundaries. An instability will therefore only establish if the total driving potential of the heat release exceeds the overall acoustic energy loss.

Despite extensive research for several decades and even though the basic principles behind thermo-acoustic instabilities are mainly understood, a reliable prediction is not given up to the present day. The reason for this lack of analytical capabilities is the complexity of the physical mechanisms behind the heat-release fluctuations. Current research activities are aiming on the application of unsteady CFD simulations.[11,23] Nevertheless, simulations of that kind are still subject to a considerable amount of uncertainty. In addition to that, the computational cost of transient

*By neglecting the mean flow impact and viscous effects.

DOI: 10.13009/EUCASS2019-592

CFD based stability analyses is often excessive and difficult to apply within the industrial development process. Besides the demonstration of stable operation within the scope of an engine qualification process the evaluation of the thermo-acoustic stability characteristics by means of full-scale testing still constitutes a major element of the industrial development process. The necessity of performing the tests at full-scale level is based upon the fact that the acoustic modes potentially interacting with the combustion process directly depend on the scale of the hardware, i.e. the thermo-acoustic conditions encountered under full-scale level cannot be investigated by means of sub-scale configurations.

The objective of the next chapters is to discuss some of the tools and techniques used to evaluate combustion stability characteristics experimentally. However, it is beyond the scope of this publication to cover all the aspects and details concerning combustion stability testing. Instead, the emphasis is placed on the measurement of the dynamic pressure inside a full-scale combustion chamber as this approach is the most accepted and widely used method for the detection and evaluation of unstable combustion in liquid rocket propulsion systems. In the course of this, the application of so-called infinite tube pressure probes is discussed in greater detail. They provide enhanced flexibility under the constrains of full-scale testing and eliminate several shortcomings of conventional measurement techniques. In the second part of the paper the reduction and analysis of the acquired test data is discussed. This includes a review of common parameters for quantifying the thermo-acoustic stability behavior.

2. Dynamic Pressure Measurement in Full-Scale Propulsion Systems

As already mentioned in the introduction, dynamic pressure measurements are the primary method for the detection of combustion instabilities and the characterization of the stability behavior. Therefore, a more detailed description of the instrumentation for this kind of measurement is given in the following.

2.1 Transducer Positioning

The location and mounting of dynamic pressure transducers within a combustion chamber is an important consideration in diagnosing thermo-acoustic instability modes. All available literature agrees that multiple dynamic pressure transducers in the combustion chamber are required in order to accurately identify the character and location of particular instability modes.[2,7,10]

Two transducers in the combustion chamber may be considered as an absolute minimum, even for flight configurations. They should be mounted at an angle of approx. 135° close to the injector face. For engine development three transducers at 0°, 135° and 270° are usually a minimum requirement and the 0° transducer should be completed with two additional transducers downstream in the combustion chamber. For baffled configurations, the downstream transducers are of increased importance. The instrumentation should be completed with several transducers in the feed system cavities i.e. domes, manifolds etc.

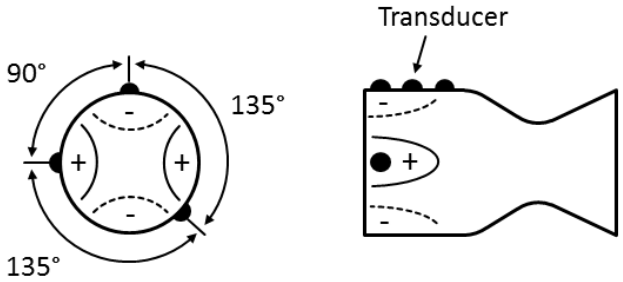

Figure 1: Positioning of dynamic pressure transducers for instability mode identification.

2.2 Transducer Transmission Behavior

To meet the frequency response requirements, flush mounted transducers are recommended in general. Flush mounted means that the pressure sensing surface of the transducer is positioned at the same level as the inner surface of the measured domain, e.g. the combustion chamber. If small back-steps or back-volumes are formed, these need to be examined for possible resonances. If resonances in the frequency range of interest are given, the mounting situation needs to be changed or countermeasures as described below should be established.

DOI: 10.13009/EUCASS2019-592

In many situations however it may be impossible to install flush-mounted transducers through the walls of the chamber (e.g. in case of regeneratively cooled chambers) or through the injector head. In these cases a small capillary is often required which connects the transducer to the measurement location. This setup however is associated with a significant reduction of the uniformity of the frequency response due to unfavorable acoustic resonances forming within the capillary. To eliminate the latter and to extend the frequency response to the required range, the application of an infinite tube measurement system is recommended.

Figure 2 illustrates a typical infinite tube probe mounted at the injection head of a liquid rocket propulsion system. The central element of the measurement system is a dynamic pressure transducer (1) connected to a T-junction (2). At the upstream end of the T-junction, a capillary tube (3) is attached. The latter must be long enough so that acoustic waves are sufficiently dissipated and the formation of standing waves (resonances) within the overall measurement system is inhibited. At the downstream end, the setup is connected to the pressure measurement location, e.g. the injector face of a liquid rocket injector head, by means of a relatively short tap-off capillary (4). In order to keep reacting, corrosive and undefined media out of the probe, the tubes are usually purged with a steady flow of inert gas which is injected at the upstream end of the long capillary tube.

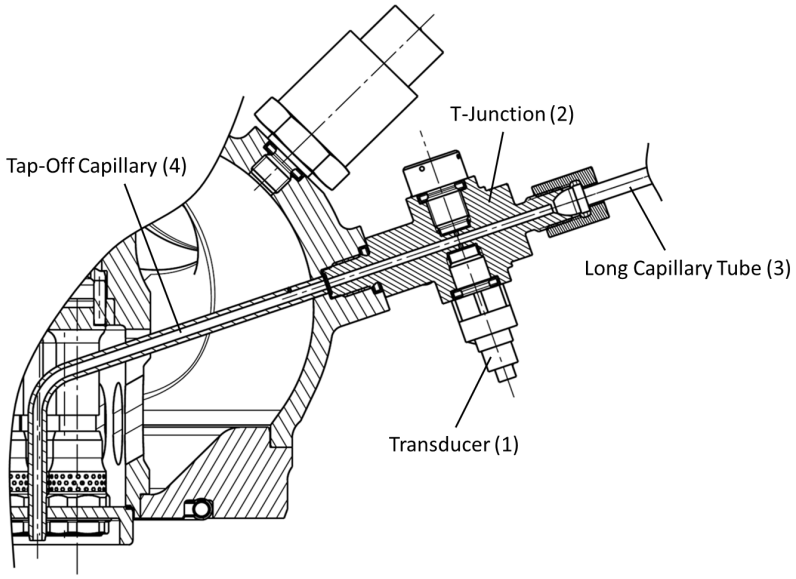

Figure 2: Infinite tube probe mounted at an injector head.

Infinite tube measurement systems are proven and well known within the gas turbine industry and community.[8,21] However there are almost no descriptions of infinite tubes utilized for rocket propulsion applications. On notable exception within this context is the application of infinite tube pressure probes within the NERVA (nuclear rocket) program during the 1960's.[22]

3. Performance Analysis of an Infinite Tube System

The transmission performance of an infinite tube probe is usually highly sensitive with respect to geometrical imperfections like small cross sectional variations and gaps or operational constrains like additional purge orifices. To ensure a sufficient measurement data quality it is therefore suggested to evaluate the performance prior to its application. In the following section an acoustic network model will be presented which allows to evaluate the impact of different operational and geometrical parameters on the performance of a probe.

3.1 Modeling Approach

An infinite tube probe is characterized by a large ratio between length and diameter of the acoustic propagation ducts. For the frequency range of interest, e.g. for oscillation frequencies $< 10kHz$, the cut-on frequency for non-longitudinal modes is not reached. This implies that the acoustic perturbations propagating within the ducts are planar waves. In this case, the acoustic performance can be analyzed by means of a so called network approach.[15,16] Here the system is divided into a variety of different acoustic elements, where each element represents the acoustic behavior of elementary

DOI: 10.13009/EUCASS2019-592

geometric components, e.g. a duct of constant cross section. Acoustic waves can enter and leave an acoustic element at the interfaces to other acoustic elements. In the frequency domain the acoustic state at these interfaces can either be described by the complex-valued acoustic pressure $\hat{p}$ and the velocity $\hat{u}$ or by the corresponding complex-valued Riemann invariants f and g.[16] The Riemann invariants or wave characteristics are related to $\hat{p}$ and $\hat{u}$ by the following relations:

$$\frac{\hat{p}}{\varrho c} = f + g\,, \tag{2a}$$

$$\hat{u} = f - g\,, \tag{2b}$$

where f denotes the Riemann invariant propagating in positive coordinate direction. Conversely g denotes the Riemann invariant propagating in negative coordinate direction. Moreover, c is the speed of sound and ϱ the mean density of the fluid. In the following the basic acoustic elements required within the acoustic analysis of an infinite tube measurement system will be discussed.

3.1.1 Duct with Losses

Within a simple duct element, acoustic waves can enter and leave the system from two sides (two-port element). The acoustic behavior is governed by two linear equations relating the incoming and outgoing waves. Neglecting the convective influence of a possible mean flow these equations in terms of the Riemann invariants can be written as:

$$f_d = \exp\left(-ikL\right) f_u\,, \tag{3a}$$

$$g_d = \exp\left(+ikL\right) g_u\,, \tag{3b}$$

where the index $(\,)_u$ denotes the Riemann invariants at the upstream port and the index $(\,)_d$ the corresponding quantities at the downstream port. L characterizes the overall or effective length of the duct. Moreover, $i = \sqrt{-1}$ is the imaginary unit and $k = \omega\Gamma/c$ is the wavenumber, where ω is the angular frequency of the acoustic oscillations. Note that k is a complex-valued quantity. If the wavenumber would be real-valued, i.e. $k = \omega/c$, only a phase change between the incoming waves and the outgoing waves would appear. In case of a complex-valued wavenumber, a change in amplitude will result in addition to the phase shift. The propagation coefficient Γ incorporates the dissipative thermo-viscous impact of the acoustic boundary layer at the duct walls. For this parameter, various modeling approaches are available within the literature. Table 1 gives on overview on some analytical expressions for the propagation coefficient. Note that all expressions depend solely on three parameters, i.e. $\Gamma = \Gamma(s, \sigma, \gamma)$, where

$$s = \frac{d}{2}\sqrt{\frac{\varrho\omega}{\mu}} \tag{4}$$

denotes the so called shear wave number,

$$\sigma = \sqrt{\frac{\mu c_p}{\kappa}} \tag{5}$$

is the square root of the Prandtl number and $\gamma = c_p/c_v$ represents the ratio of the specific heats. Within above expressions, d specifies the inner diameter of the duct. Moreover, the dynamic viscosity is denoted by μ and the thermal conductivity by κ.

3.1.2 Network Junctions with Area Change

Acoustic junctions are characterized by one or more incoming connections and one or more outgoing connections. In the scope of this analysis, acoustic junctions are treated as compact, which implies that the effective geometric length of this element is small with respect to the acoustic wavelength. Moreover, the convective impact of a possible mean flow as well as associated acoustic losses are neglected. To fully describe the acoustic behavior of acoustic multi-ports, a system of N equations is required, where N equals the total number of in- and outgoing connections. Assuming the continuity of the acoustic pressure and the conservation of mass, the required governing equations can be written in terms of the Riemann invariants as follows:

$$\sum_{j=1}^{N} A_j(f_j - g_j) = 0\,, \tag{6a}$$

$$f_j + g_j - f_{j+1} - g_{j+1} = 0 \quad \text{for} \quad j = 1...N-1\,, \tag{6b}$$

with A_j denoting the the cross-sectional area at connection port j.

DOI: 10.13009/EUCASS2019-592

Author	Year	Expression
Kirchhoff[13]	1868	$\Gamma = 1 + \left(\frac{1-i}{\sqrt{2}}\right)\left(\frac{\gamma+\sigma-1}{\sigma s}\right)$
Rayleigh[18]	1896	$\Gamma = 2(1-i)\sqrt{\frac{\gamma}{s^2}}$
Ronneberger[20]	1975	$\Gamma = 1 + \left(\frac{1-i}{\sqrt{2}}\right)\left(\frac{\gamma+\sigma-1}{\sigma s}\right) - \frac{i}{s^2}\left(1 + \frac{\gamma-1}{\sigma} - \frac{\gamma^2-\gamma}{2\sigma^2}\right)$
Zwikker and Kosten[24]	1949	$\hat{\Gamma} = \sqrt{-\frac{J_0(s\sqrt{-i})}{J_2(s\sqrt{-i})}}\sqrt{\gamma + (\gamma-1)\frac{J_2(s\sigma\sqrt{-i})}{J_0(s\sigma\sqrt{-i})}}$

Table 1: Overview on common analytical expressions for the propagation coefficient Γ. J_m is the m-th order Bessel function of the first kind.

3.1.3 Additional Purge Orifice

According to Figure 2, the tap-off capillary within the shown injector head includes a small purge orifice. Note that this orifice is not related with the infinite tube design, but has been part of the original dynamic pressure measurement concept. Neglecting compressibility and inertial effects, the following linearized relation between pressure perturbations upstream of the orifice $\hat{p}$, the unsteady flow velocity within the vena-contracta of the orifice $\hat{u}_{vc}$ and the mean pressure difference across the orifice Δp can be derived:

$$\frac{\hat{p}}{\hat{u}_{vc}} = \sqrt{2\varrho\Delta p} \tag{7}$$

This expression together with the conservation of mass and the continuity of the dynamic pressure across the acoustic element provides the basis for the following governing equations in terms of the Riemann invariants:

$$f_u + g_u - f_d - g_d = 0\,, \tag{8a}$$
$$(1-K)f_u - (1+K)g_u - f_d + g_d = 0\,, \tag{8b}$$

with

$$K = \frac{C_c A_{ori}}{A_d}\left(\frac{\varrho c}{\sqrt{2\varrho\Delta p}}\right) \tag{9}$$

where $C_c \approx 0.64$ is the coefficient of flow contraction and A_{ori} and A_d denote the cross sectional area of the orifice and the duct, respectively.

3.1.4 Model Assembly and Method of Solution

According to the acoustic network approach, the infinite tube probe shown in Figure 2 is decomposed into a system of acoustic elements. Figure 3 shows a sketch of the basic network structure.

The acoustic properties of the reflection elements are expressed in terms of a so called reflection coefficient r which relates the amplitude of the reflected wave to the amplitude of the incoming wave. For the analysis perfect frequency independent reflection behavior is assumed, i.e.: $r_1 = f_1/g_1 = 1$ and $r_2 = g_6/f_6 = 1$. Note that this is actually a conservative assumption. With perfect reflection, the loss of acoustic energy will be minimized leading to an overprediction of potential acoustic resonances inside the infinite tube system. The network model is acoustically excited at the measurement location. Here, a constant velocity boundary condition $f_{10} - g_{10} = \hat{u}_{10}$ is imposed. It should be mentioned that the specific type of excitation (pressure or velocity) is arbitrary. Moreover the amplitude of the excitation is arbitrary, too, due to the fact that the model is based on linear acoustics.

The network model as shown within Figure 3 includes a total number of $N = 2M = 20$ unknown Riemann invariants. For the determination of these unknowns the governing equations of each acoustic element within the network together with the specified boundary conditions can be combined into a single matrix equation for the whole

DOI: 10.13009/EUCASS2019-592

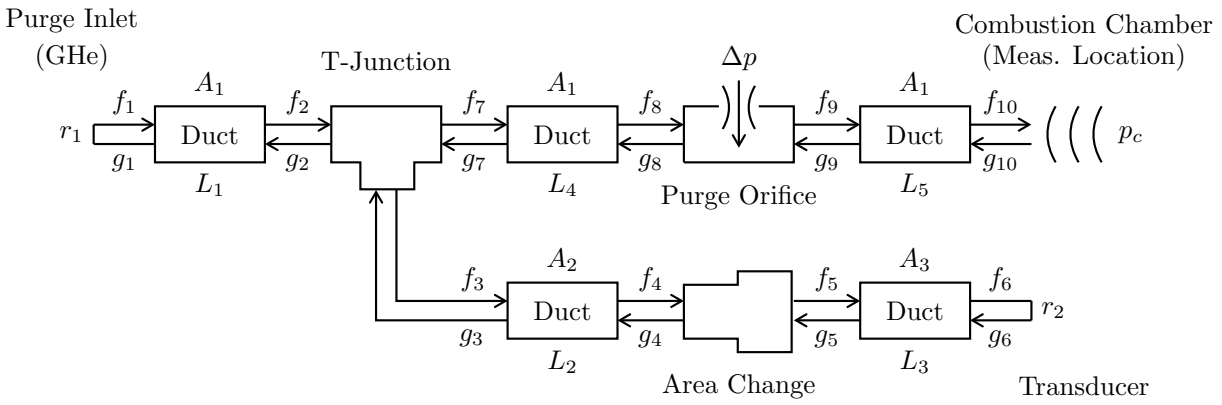

Figure 3: Acoustic network structure of the infinite tube probe shown in Figure 2

system:

$$\begin{bmatrix} a_{11}(\omega) & \cdots & a_{1N}(\omega) \\ \vdots & & \vdots \\ a_{M1}(\omega) & \cdots & a_{MN}(\omega) \end{bmatrix} \begin{bmatrix} f_1 \\ g_1 \\ \vdots \\ f_M \\ g_M \end{bmatrix} = \begin{bmatrix} b_1 \\ \vdots \\ b_M \end{bmatrix} \tag{10}$$

where $a_{ij}(\omega)$ are the frequency dependent components of the system matrix, $[f_1, g_1 \ \ldots \ f_M, g_M]^T$ is the vector of unknown Riemann invariants and b_j the RHS of the linear system of equations. In the course of this analysis, the matrix equation is assembled and solved within the MATLAB®environment.

The performance of a dynamic pressure measurement system is usually expressed in terms of the transfer function $H(\omega) = \hat{p}_T/\hat{p}_c$ which relates the pressure at the measurement location $\hat{p}_c \sim f_{10} + g_{10}$ to the pressure at the transducer $\hat{p}_T \sim f_6 + g_6$. To extract the transfer function from the network model the coefficients of the system matrix a_{ij} are evaluated for a given frequency range of interest and the corresponding matrix equations are solved for the unknown Riemann invariants.

3.2 Model Results

Figure 4 illustrates the calculated transfer behavior of the probe shown in Figure 2. The results have been obtained with the thermo-viscous dissipation model of Zwikker and Kosten[24] and are depicted for two different pressure levels: ambient and 100bar. In both cases the magnitude response of the dynamic pressure probe $|H(\omega)|$ is largely flat up to frequencies of approximately 1kHz. For frequencies exceeding the latter limit, an increasing oscillatory behavior can be noticed in addition to an overall decrease of the magnitude level. The oscillations in terms of the magnitude response can be traced back to acoustic resonances inside the probe owing to acoustic reflections at geometrical imperfections, i.e. at the branching purge orifice and the transducer attachment passage. Note that the amplitude of the resonances is a clear function of the pressure level. In general increased pressure results in lower kinematic viscosity $\nu = \mu/\varrho$ and as a consequence in higher shear wave numbers $s \sim \sqrt{\omega/\nu}$. This finally leads to a significant reduction of the thermo-viscous dissipation which has a direct impact on the height of the resonance peaks. The phase angle between the pressure at the measurement location p_c and the pressure at the transducer p_T increases continuously and becomes significant for frequencies at which the tap-off section represents multiple wavelengths. The variation of the phase angle is almost linear indicating a constant time delay

$$\tau = -\frac{d\arg(H)}{d\omega} \approx \frac{L_4 + L_5}{c} \tag{11}$$

between the measurement location and the transducer. Contrary to the magnitude, no visual impact of the absolute pressure level on the phase response of probe is observed. Besides geometry, the phase angle is primarily influenced by the local speed of sound in the purge fluid, where the latter is largely independent of pressure.

To assess the quality of the model, acoustic measurements at ambient conditions have been carried out. In the course of this, the infinite tube probe has been excited in a frequency range between $1.5kHz$ and $4.5kHz$ by means

DOI: 10.13009/EUCASS2019-592

of an acoustic compression driver. The frequency response was then obtained by correlating the signal of the probe transducer with a reference measurement at the location of the excitation source. According to Figure 4, the predicted characteristics agree well with the obtained measurement data.

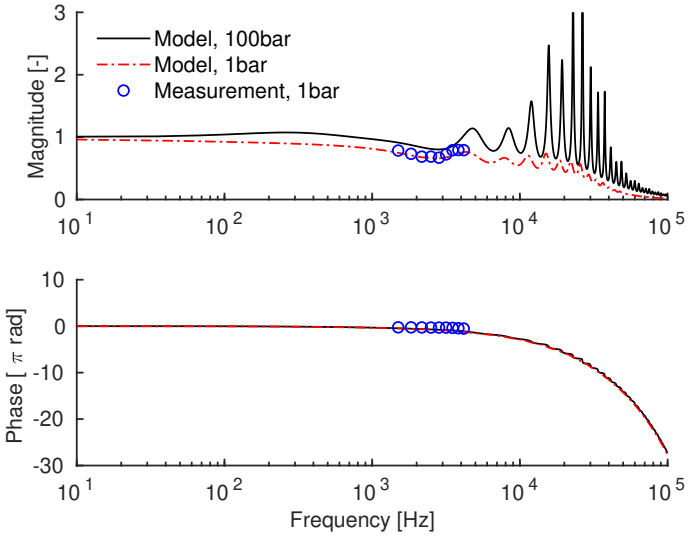

Figure 4: Calculated transfer behavior and comparison with acoustic measurement data

3.3 Full Scale Experience

In the previous section, it was found that the acoustic network approach is capable of accurately predicting the transmission performance of an infinite tube probe. In the following, the performance under hot and full-scale conditions will be discussed. Figure 5 illustrates the dynamic pressure spectra for three different measurement setups in a LRE full-scale application. The spectra are presented in terms of a normalized frequency Ω which allows to better identify the dominant acoustic chamber modes within the data:

$$\Omega = \frac{\omega r_c}{c} \tag{12}$$

where r_c denotes the radius of the combustion chamber and c is the characteristic speed of sound of the hot combustion product. With this definition, the transverse acoustic chamber modes are indicated by the roots of the m-th order Bessel function derivative Ω_{mn}, i.e. the first two tangential chamber modes T1 and T2 are characterized by a normalized theoretical resonance frequency of $\Omega_{10} = 1.841$ and $\Omega_{20} = 3.054$, respectively.

The spectrum shown in Figure 5a has been measured inside a capacitively cooled combustion chamber configuration by means of a flush mounted dynamic pressure transducer. It is composed of at least three characteristic regions with increased spectral amplitudes. By comparing the measured spectrum with the analytical transverse mode frequencies at least two of these regions can be identified as resonance peaks of the first and second tangential combustion chamber mode. The third region lies below the cut-on frequency of the transverse modes ($\Omega < 1.841$). Numerical simulations however have shown that this region is likely the spectral contribution of the first and second longitudinal combustion chamber mode.

The data of Figure 5b corresponds to a regeneratively cooled version of the previous combustion chamber. Due to geometrical constrains an integration of flush mounted transducers into the design was not possible. Instead, an infinite tube probe has been utilized in order to accurately measure the dynamic content of the combustion chamber pressure. Compared to the spectrum of the flush mounted transducer only minor differences can be noticed. The latter are mainly visible in terms of the local amplitude levels. The overall picture of the spectrum is however fully preserved. It should also be mentioned that the operating conditions of the combustion chamber are not fully identical in both cases, i.e. the differences are not necessarily introduced by the infinite tube probe but may also result from slightly different operating condition.

Figure 5c finally illustrates the consequences of connecting the transducer to the combustion chamber by means of a capillary without an infinite tube. Due to the highly reflecting termination, an acoustic resonator is formed whose resonance peaks interfere with the actual combustion chamber spectrum. In many cases, the artificial resonance peaks dominate the overall spectrum making the data useless for further stability analyses. This clearly demonstrates the necessity of advanced measurement techniques like infinite tube probes.

DOI: 10.13009/EUCASS2019-592

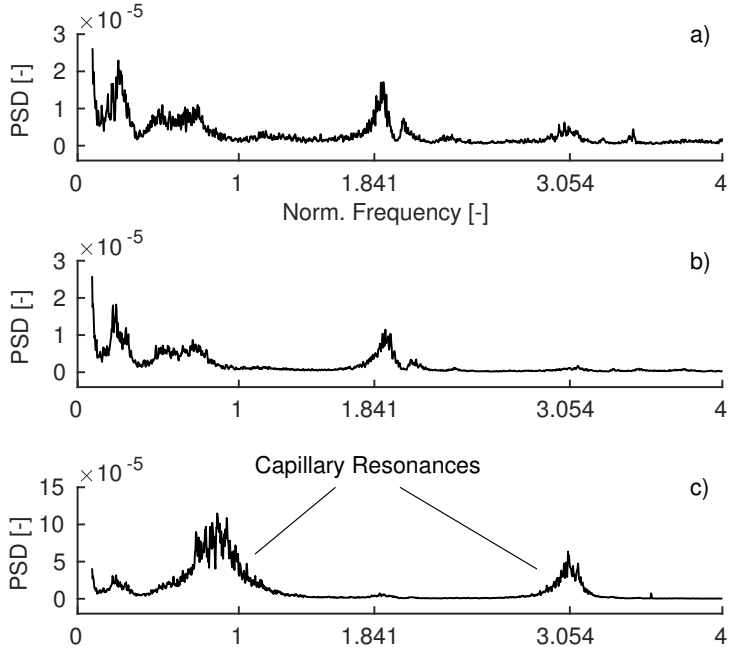

Figure 5: Power spectrum density (PSD) of the dynamic chamber pressure for three different measurement setups: flush mounted transducer a), infinite tube probe b), tap-off capillary without infinite tube c).

4. Evaluation of Stability

The knowledge of accurate dynamic pressure data facilitates a conclusive evaluation of the thermo-acoustic stability characteristics. In the following sections an overview on common methods for stability assessment and test data evaluation is given. In the course of this, important quantities for the characterization and interpretation of hot-firing test data are presented and discussed. Please note however, that most of the subsequent information is related to the linear or spontaneous stability only.

4.1 Quantification of Thermo-acoustic Stability

4.1.1 Root-Mean-Square

The root-mean-square (RMS) value of dynamic pressure is probably the most common measure for the quantification of engine stability. It is common practice to examine this quantity in order to distinguish between stable and unstable engine operation. In general, root-mean-square can be formulated both in the time and frequency domain. In the time domain the RMS of an unsteady quantity $p' = p - \bar{p}$, where $\bar{p}$ is the temporal mean of the instantaneous signal p, is defined as follows:

$$p'_{RMS} = \sqrt{\frac{1}{N} \sum_{t_i=t_1}^{t_2} p'(t_i)^2} \tag{13}$$

where N denotes the total number of samples within the evaluation window. Note that the unsteady component p' is usually high- or bandpass filtered in order to quantify the contribution of the thermo-acoustic fluctuation on the overall combustion roughness. Thereby, the cut-on frequency of the filter is selected to be slightly below the resonance frequency of the lowest acoustic chamber mode, usually the first longitudinal mode. As an alternative to the time domain, the root-mean-square may also be determined from the power spectrum density PSD of the signal by means of the following relation:

$$p'_{RMS}(f_1, f_2) = \sqrt{\Delta f \sum_{f_i=f_1}^{f_2} \mathrm{PSD}(f_i)} \tag{14}$$

where Δf is the spectral resolution and f_1 and f_2 denote the lower and upper frequency limit for the root-mean-square determination. Note that both the time and frequency domain method are equivalent with respect to the final result. The primary advantage of the frequency domain based method is the avoidance of the pre-filter step.

DOI: 10.13009/EUCASS2019-592

4.1.2 Spectral Entropy

Spectral entropy is a measure for the distribution of a signal's frequency components and provides a way to quantify how complex, organized or noise-like a signal is. A high spectral entropy level indicates that the spectrum has a similar amount of power in all frequency bands. Conversely a low spectral entropy indicates that the signal power is concentrated in a relatively small number of frequency bands. In addition to the root-mean-square amplitude of the dynamic chamber pressure, the spectral entropy may be utilized as another indicator for unstable combustion chamber operation. The normalized form of the spectral entropy NSE (approaching 1.0 for Gaussian white noise) in the frequency range between f_1 and f_2 is calculated as follows:

$$\mathrm{NSE}(f_1, f_2) = -\frac{\sum_{f_i=f_1}^{f_2} P(f_i) \ln P(f_i)}{\ln N} \tag{15}$$

where the "probability" $P(f_i)$ with $\sum_{f_i} P(f_i) = 1$ is given as:

$$P(f_i) = \frac{\mathrm{PSD}(f_i)}{\sum_{f_i=f_1}^{f_2} \mathrm{PSD}(f_i)} \, . \tag{16}$$

Spectral entropy may also be applied in order to distinguish between unstable and rough combustion. Thus rough combustion is characterized by increased dynamic pressure fluctuations in combination with spectral entropy levels exceeding the values of unstable combustion.

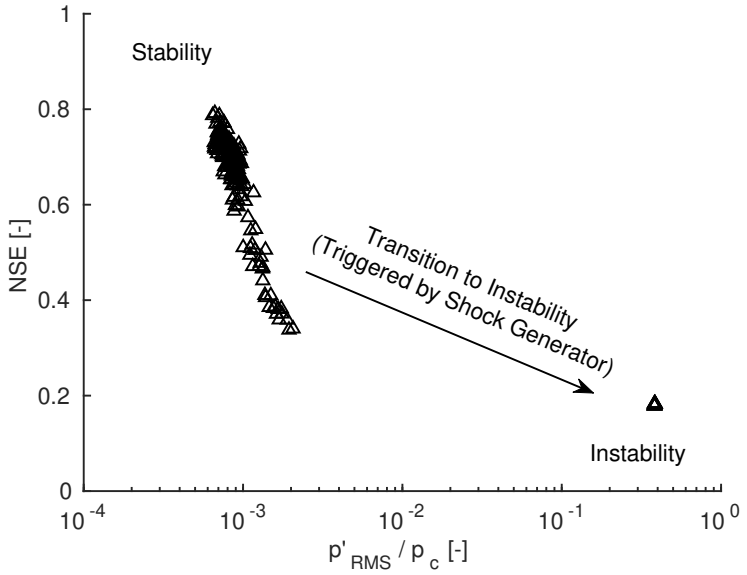

Figure 6: Typical root-mean-square dynamic pressure and normalized spectral entropy levels encountered during stable and unstable combustion chamber operation.

4.1.3 Characteristic Damping

The rate at which acoustic disturbances are damped in a stable combustion chamber has been proposed as a potential measure for determining the proximity to the spontaneous stability limit.[7,10,14] Considering a disturbance of sufficiently low amplitude such that nonlinear effects are negligible the response of the chamber pressure at a fixed location to some perturbation can be formulated as a sum of expressions of the form

$$p'(t) = A \exp(-\alpha t) \cos(\omega_r t + \phi) \tag{17}$$

where $p'(t)$ denotes the contribution of a particular resonance mode with angular resonance frequency ω_r to the overall chamber pressure response. The temporal evolution of the disturbance amplitude is defined by the damping coefficient α which is a lumped parameter including both potential excitation effects due to the combustion process as well as the inherent acoustic damping of the system. The damping coefficient α is a dimensional quantity with units s^{-1} expressing the absolute speed of the exponential amplitude decay. To evaluate the significance of the damping, the latter has to be put into relation with the characteristic time scale of the oscillation. This finally leads to characteristic non-dimensional quantities commonly used within the assessment of LRE stability.

DOI: 10.13009/EUCASS2019-592

Quality Factor The quality factor Q is a non-dimensional damping measure which is widely used within the context of oscillators and resonators. It is usually defined in the frequency domain as the ratio between the resonance angular frequency of a particular mode ω_r and the corresponding full width at half-maximum bandwidth $\Delta\omega_{3dB}$. Moreover it can be expressed as π-times the ratio between the oscillation frequency and the damping coefficient, i.e.:

$$Q = \frac{\omega_r}{\Delta\omega_{3dB}} = \frac{\pi f_r}{\alpha} \, . \tag{18}$$

Higher Q values indicate a lower rate of relative energy loss. With respect to thermo-acoustic stability this means that a system would operate closer to the stability limit. Conversely low values of Q correspond with increased rates of energy loss indicating higher stability margins with respect to linear or spontaneous instabilities. For $Q = 0.5$ the critical amount of damping is reached. In this case as well as for $Q < 0.5$ the dynamic system would no longer be able to oscillate (critically or overdamped state).

Oscillation Decrement The oscillation decrement δT is another non-dimensional stability or damping measure which is often found in the Russian literature on thermo-acoustic stability of LRE.[7] It is based on the same principles as the quality factor and as a consequence the oscillation decrement can be converted into the quality factor and vice versa:

$$\delta T = \frac{\pi \, \Delta\omega_{3dB}}{\omega_r} = \frac{\pi}{Q} = \frac{\alpha}{f_r} \, . \tag{19}$$

In case of the oscillation decrement, higher values of δT are linked with an increased amount of stability margin whereas an operation towards the stability limit would be indicated by values of δT approaching zero.

4.2 Determination of the Characteristic Damping from Natural Disturbances

4.2.1 Half-Power Bandwidth Method and Lorentzian Fitting

A common method for the determination of the characteristic damping during steady-state engine operation is to use the ambient combustion noise as a natural disturbance source. It is assumed that the spectral content of the natural excitation source is of larger bandwidth than the response characteristics of the combustion chamber in the vicinity of the resonance frequencies being studied. Under this assumption the so-called half-power bandwidth method can be applied.[10] Here, the damping is determined by directly measuring ω_r and $\Delta\omega_{3dB}$ of a particular resonance peak in the amplitude spectrum of the dynamic chamber pressure (Figure 7).

Since the half-power bandwidth method relies only on three points, significant errors can be introduced if the response data has only a very limited frequency resolution and/or the analyzed peak is superimposed with other resonance modes. In this case, it is recommended to fit an analytical response function to the measurement data. The response function $\hat{p}(\omega)$ that corresponds with an exponentially damped simple harmonic oscillation is a so-called Lorentzian curve of the form:

$$\frac{\hat{p}(\omega)}{\hat{p}(\omega = \omega_r)} = \frac{\alpha^2}{\alpha^2 + (\omega_r - \omega)^2} = \frac{\gamma^2}{\gamma^2 + (f_r - f)^2} \tag{20}$$

where $\gamma = \alpha/2\pi$ and $\hat{p}(\omega = \omega_r) = |\hat{p}|_{max}$ denotes the response maximum. By fitting above profile to the measured amplitude spectrum of the dynamic chamber pressure, both the damping coefficient α and the corresponding resonance frequency f_r are determined with an accuracy that is usually superior to the simple half-power bandwidth method.

4.2.2 Parametric Modelling

This approach is based on the assumption that the temporal evolution of the dynamic chamber pressure can be described by means of a parametric time series model such as the auto-regressive model (AR).[5,12] Mathematically, an AR model of order p can be expressed as:

$$x[n] = \sum_{k=1}^{p} a_k x[n-k] + e[n] \tag{21}$$

where $x[n]$ is the value of the time series at sample point n, a_k are the real valued model coefficients and $e[n]$ represents a white noise error term which is independent of the past samples. An AR model may also be considered as a digital infinite impulse response filter (IIR) whose response function in the z-domain is given as:

$$H(z) = \frac{1}{1 - \sum_{k=1}^{p} a_k z^{-k}} \tag{22}$$

DOI: 10.13009/EUCASS2019-592

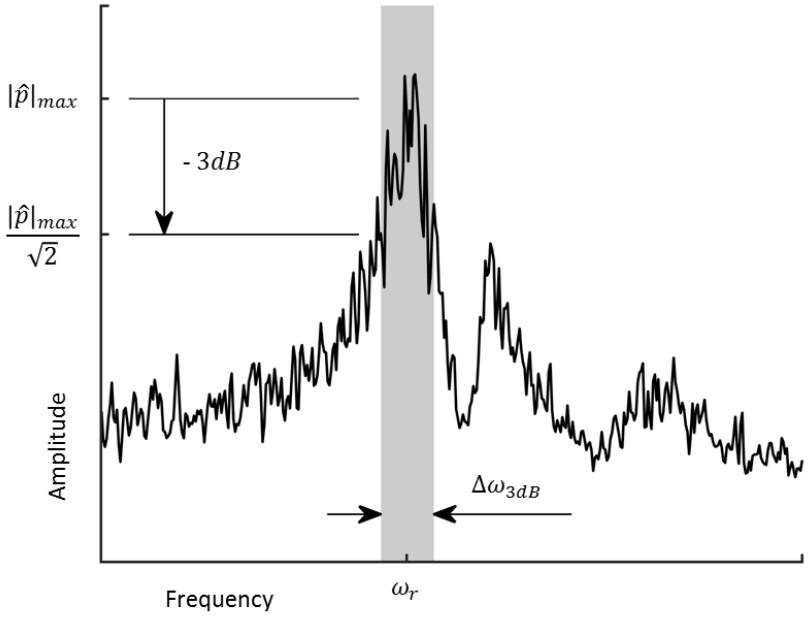

Figure 7: Characteristic damping evaluation of a spectral peak by means of the bandwidth method.

The complex roots $z_i^{\times}$ of the response function correspond with the resonance peaks of the signal spectrum. The resonance frequencies $\omega_i = \mathrm{Im}(s_i^{\times})$ and the associated damping rates $\alpha_i = \mathrm{Re}(s_i^{\times})$ are obtained by transforming the roots from the discrete z domain to the continuous Laplace domain, i.e.

$$s_i^{\times} = \frac{\ln(z_i^{\times})}{\Delta t} \tag{23}$$

where Δt is the constant sampling time. To estimate the auto-regressive model coefficients a_k from the input time series, a variety of different algorithms have been proposed such as Yule-Walker, least-squares and Burg-type estimators. Care shall be taken in case of Yule-Walker as this method has shown to be erroneous for small data segments.[6] An important aspect of the parametric modelling approach is the correct choise of the model order p. The order may be chosen according to the total number of acoustic resonance peaks wihin the frequency range of the input signal. However, it is often more appropriate to apply one of the various order selection criteria like the Akaike Information Criterion (AIC), Final Prediction Error (FPE) or the Minimum Description Length (MDL).[3,4,19]

Figure 8 illustrates an example for modal characteristics which have been estimated from the dynamic pressure signal of a full-scale hardware by means of parametric modeling. The results are shown in terms of a scatter plot where each data point is related with the characteristics during an evaluation window of 100ms. Note that the points are clustered around three regions where the regions represent the linear stability characteristics of the first and second tangential thrust chamber mode as well as a feed-system-coupled oscillation, respectively.

4.3 Common Criteria for Sustained Stability

Due to the large number of factors affecting the stability characteristics of liquid rocket propulsion systems it is often impossible to define exact quantitative criteria which guarantee thermo-acoustic stability under all circumstances. Several examples are known where sudden instabilities have been encountered despite extensive testing with stable operation prior to the incident.[10] Nevertheless, experience gained within numerous thrust chamber firings allows to define at least some order of magnitude criteria. If these criteria are fulfilled a high probability for sustained thermo-acoustic stability can be expected.

At least two order of magnitude criteria have been published within the common literature on LRE combustion stability. According to Dranovsky,[7] combustion chambers with stable operating processes exhibit oscillation decrements in the range of

$$\delta T \approx 0.1 \ldots 0.3 \, . \tag{24}$$

DOI: 10.13009/EUCASS2019-592

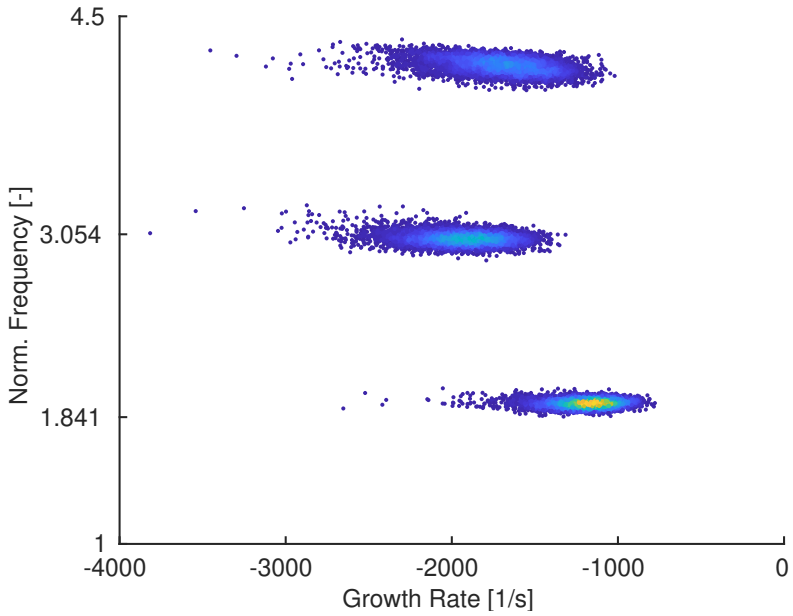

Figure 8: Scattering of linear damping rates and associated frequencies during a long duration full-scale test (color corresponds with data point density). The modal damping rates have been estimated from the dynamic chamber pressure signal by means of parametric modeling.

Another criterion has been published within the US guidelines on combustion stability specification and verification procedures.[1,2] Contrary to Dranovsky[7] this criterion is based on a maximum allowable damping time

$$t_D \leq 1.25s\sqrt{\frac{1Hz}{f_r}}. \tag{25}$$

For potentially unstable frequencies in the range of $f_r \approx 2\ldots10kHz$ and by assuming that t_D represents the elapsed time required for a disturbance to decay to 10% of its initial amplitude, limiting oscillation decremens in the range of $\delta T \geq 0.02\ldots0.04$ would be attained. Note that this limit significantly exceed the recommendation of Dranovsky, i.e. the criterion stated by CPIA[1,2] would be substantially weaker. It should be mentioned that the US criterion is based on experience for the allowable time, with an acceptable margin, that an oscillation can be present without the engine encountering damage. Furthermore the criterion has been formulated for finite disturbances (dynamic stability) whereas the Dranovsky recommendation is only given for "soft" excitation.[7]

5. Summary and Conclusions

A short overview on current methods for assessing the thermo-acoustic stability characteristics of liquid rocket propulsion systems has been given. Prerequisite for the successful application of these methods is an accurate measurement of the dynamic pressure fluctuations inside the combustion chamber. It has been shown that infinite tube pressure probes are capable of providing the necessary data under the constrains of of full-scale testing.

References

[1] CPIA Publication 247, Guidelines for Combustion Stability Specifications and Verification Procedures for Liquid Propellant Rocket Engines, 1973.

[2] CPIA Publication 655, Guidelines for Combustion Stability Specifications and Verification Procedures for Liquid Propellant Rocket Engines, 1997.

[3] H. Akaike. Fitting autoregressive models for prediction. *Annals of the Institute of Statistical Mathematics*, 21(1):243–247, 1969.

DOI: 10.13009/EUCASS2019-592

[4] H. Akaike. Statistical predictor identification. *Annals of the Institute of Statistical Mathematics*, 22(1):203–217, 1970.

[5] F. E. C. Culick. Unsteady motions in combustion chambers for propulsion systems. RTO AGARDograph AG-AVT-039, North Atlantic Treaty Organization (NATO), 2006.

[6] M. J. L. de Hoon, T. H. J. J. van der Hagen, H. Schoonewelle, and H. van Dam. Why Yule-Walker schould not be used for autoregressive modelling. *Annals of Nuclear Energy*, 23:1219–1228, 1996.

[7] M. L. Dranovsky, V. (Ed.) Yang, F. (Ed.) Culick, and D. (Ed.) Talley. *Combustion Instabilities in Liquid Rocket Engines: Testing and Development Practices in Russia*. AIAA Progress in Astronautics and Aeronautics, Volume 221, 2007.

[8] D. R. Englund and W. B. Richards. The infinite line pressure probe. Technical Report NASA-TM-83582, National Aeronautics and Space Administration (NASA), 1984.

[9] D. M. Harland and R. D. Lorenz. *Space Systems Failures, Disasters and Rescues of Satellites, Rockets and Space Probes*. Springer Praxis Publishing Ltd., 2005.

[10] D. T. Harrje and F. H. (Eds.) Reardon. Liquid propellant rocket combustion instability. Technical Report SP 194, National Aeronautics and Space Administration (NASA), 1972.

[11] M. E. Harvazinski, R. M. Gejji, D. G. Talley, M. R. Orth, W. E. Anderson, and T. L. Pourpoint. Modeling of transverse combustion instability. In *AIAA Scitech 2019 Forum, January 7-11, 2019, San Diego, CA, USA*, number AIAA 2019-1732, 2019.

[12] R. O. Hessler, R. L. Glick, R. Bertelè, D. Cedro, G. Fiorentino, and L. T. DeLuca. Passive stability measurements in a model rocket chamber. In *Space Solid Propulsion, November 21-24, 2000, Rome, Italy*, 2000.

[13] G. Kirchhoff. Ueber den einfluss der wärmeleitung in einem gase auf die schallbewegung. *Poggendorfer Annalen*, 134:177–193, 1868.

[14] T. Lieuwen. Online combustor stability margin assessment using dynamic pressure data. *Journal of Engineering for Gas Turbines and Power*, 127(3):478–482, 2005.

[15] M. L. Munjal. *Acoustics of Ducts and Mufflers*. Wiley and Sons, 1987.

[16] W. Polifke, J. van der Hoek, and B. Verhaar. Everything you always wanted to know about f and g. Technical report, ABB Corporate Research, 1997.

[17] J. W. S. B. Rayleigh. *The Theory of Sound*, volume 1. Macmillan, 1894.

[18] J. W. S. B. Rayleigh. *The Theory of Sound, 2nd ed.*, volume 2. Macmillan, 1896.

[19] J. Rissanen. Modeling by the shortest data description. *Automatica*, 14:465–471, 1978.

[20] D. Ronneberger. Genaue messung der schalldämpfung und der phasengeschwindigkeit in durchströmten rohren im hinblick auf die wechselwirkung zwischen schall und turbulenz. Habilitation Thesis, Universität GÃ¶ttingen, 1975.

[21] M. Salikuddin, R. H. Burrin, and W. H. Brown. Design and characterization of a high temperature and high frequencyinfinite-line pressure probe. In *12th AIAA, Aeroacoustics Conference, April 10-12, 1989, San Antonio, TX, USA*, number AIAA 2004-456, 1989.

[22] R. D. Samuelson. Pneumatic instrumentation lines and their use in measuring rocket nozzle pressure. Technical Report RN-DR-0124, Aerojet-General Corporation, 1967.

[23] A. Urbano, L. Selle, G. Staffelbach, B. Cuenot, T. Schmitt, S. Ducruix, and S. Candel. Exploration of combustion instability triggering using Large Eddy Simulation of a multiple injector liquid rocket engine. *Combustion and Flame*, 169:129–140, 2016.

[24] C. Zwikker and C. W. Kosten. *Sound Absorbing Materials*. Elsevier Science Ltd, 1949.